Soils and Foundations 2016;56(1):152–159

HOSTED BY

ELSEVIER

CrossMark

The Japanese Geotechnical Society

Soils and Foundations

www.sciencedirect.com

journal homepage: www.elsevier.com/locate/sandf

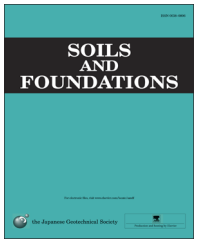

Assessing the quasi-static conditions for shearing in granular media within the critical state soil mechanics framework

J.C. Lopera Perez[a], C.Y. Kwok[a,*], C. O'Sullivan[b], X. Huang[a,b,c], K.J. Hanley[b]

[a]Department of Civil Engineering, The University of Hong Kong, Haking Wong Building, Pokfulam Road, Hong Kong
[b]Department of Civil and Environmental Engineering, Imperial College London, Skempton Building, London SW7 2AZ, UK
[c]Department of Geotechnical Engineering, Tongji University, Shanghai 200092, China

Received 4 February 2015; received in revised form 29 July 2015; accepted 16 September 2015
Available online 19 February 2016

Abstract

There has been a marked increase in the use of the discrete element method (DEM) in geomechanics in recent years. The way in which DEM simulations are set up can have a noticeable influence on the observed response. The conditions for quasi-static shearing in DEM simulations of granular materials were studied here within the critical-state framework of the soil behaviour. Thirty-two constant-p' triaxial simulations were carried out from which the critical-state relationships were defined in the void ratio-mean effective stress and deviator fabric-mechanical coordination number planes. Clear trends were observed for the void ratio, the coordination number, and the deviatoric fabric at the critical state as the inertial number, I, was varied. The critical state relationships were aligned along distinct loci for each value of I. The critical state framework was used to show that there is an upper bound to the I values below which the simulation is quasi-static and that the observed behaviour is independent of the strain rate. The parameter I was shown to be a useful measure for assessing the quality of quasi-static DEM simulations.

Keywords: Discrete element modelling; Fabric/structure of soils; Particle-scale behaviour; Triaxial tests (IGC: D3/D6/E13)

1. Introduction

Significant, fundamental insight into the mechanics underlying the observed complex, non-linear response of granular materials can be gained via numerical simulations using the Discrete Element Method (DEM) (Cundall and Strack, 1979). Under quasi-static conditions, there is no strain rate dependency. Therefore, establishing general guidelines for the strain rate and material properties required to accomplish this is important. Cundall and Strack (1979) suggested that in order to achieve quasi-static conditions, a strain rate should be chosen such that the inertial forces are smaller than the contact forces. In practice, however, a parametric study is often carried out to select the strain rate below which a consistent response is obtained. Many published research studies do not clearly state the value of the adopted strain rate. Hanley et al. (2013) showed that there is a clear sensitivity of the stress–strain response of constant-volume DEM simulations to the strain rate; thus, it is evident that attention should be paid to this matter.

The transition from the quasi-static regime, where the inertial effect is negligible, to the dynamic regime, where the inertial effect is significant, has been studied widely both numerically (MiDi, 2004; da Cruz et al., 2005; Hatano, 2007;

*Correspondence to: Room 521, Haking Wong Building, Department of Civil Engineering, The University of Hong Kong, Pokfulam Road, Hong Kong. Tel.: +852 2859 2655; fax: +852 2559 5337.
E-mail address: fiona.kwok@hku.hk (C.Y. Kwok).
Peer review under responsibility of The Japanese Geotechnical Society.

http://dx.doi.org/10.1016/j.sandf.2016.01.013

Notations

d	particle diameter
D	dilatancy $D=d\varepsilon_v/d\varepsilon_q$
e	void ratio
e_0	initial void ratio
e_{cs}	void ratio at the critical state
G	particle shear modulus
I	inertial number
p'	mean effective stress
p_0'	mean effective stress after isotropic compression
q	deviatoric stress
Z_m	mechanical coordination number
Γ	intercept of the critical state line in the $e-(p'/p_a)^{0.7}$ space with axis $p'=0$
$\dot{\varepsilon}$	strain rate
ε_1; ε_2; ε_3	major, intermediate and minor principal strains ($\varepsilon_2=\varepsilon_3$)
ε_v	volumetric strain
η	stress ratio $\eta=(q/p')$
ε_q	shear strain $\varepsilon_q=2/3(\varepsilon_1-\varepsilon_3)$
λ	slope of the critical state line in the $e_{cs}-(p'/p_a)^{0.7}$ space
μ	inter-particle friction coefficient
ν	particle Poisson's ratio
ρ	particle density
σ'_1; σ'_2; σ'_3	major, intermediate and minor principal stresses ($\sigma'_2=\sigma'_3$)
$(\Phi_1-\Phi_3)$	deviatoric fabric

Agnolin and Roux, 2007; Peyneau and Roux, 2008; Koval et al., 2009; Radjai and Dubois, 2011; Gimbert et al., 2013; Azema and Radjai, 2014) and experimentally (Kuwano et al., 2013). Many of these studies used a dimensionless parameter called the inertial number, $I=\dot{\varepsilon}d\sqrt{\frac{\rho}{p'}}$, to identify different flow regimes, where $\dot{\varepsilon}$ is the shear rate, d is the mean size of grains in the assembly, ρ is the grain density, and p' is the mean effective stress (da Cruz et al., 2005). I quantifies the inertia effects by considering the ratio of the inertial forces to the imposed forces. Small values for I correspond to a quasi-static regime, intermediate values for I indicate a dense flow regime, and large values for I indicate a collisional dynamic regime (da Cruz et al., 2005). Prior studies have focussed on determining the characteristic values for I that separate these quasi-static, dense flow, and dynamic regimes, often using plane shear tests. For example, the boundary between the quasi-static and the dense flow regimes varies between $I<1e-4$ and $I<1e-1$ (Macaro and Utili, 2012; Kuwano et al., 2013). The objectives of this study are to extend these findings from a soil mechanics perspective by investigating the effect of I on the critical state locus (CSL), at both macro and particle-scales, and to propose an upper limit for I that defines the quasi-static state regime when simulating soil mechanics element tests.

DEM simulations of triaxial tests under a range of initial densities and confining pressures were performed. In each simulation, I was maintained constant throughout the shearing stage. Critical state lines in the $e-(p'/p_a)^{\alpha}$ plane were identified for each I value considered. The critical state relationships were also explored at the particle scale by considering the coordination number and the deviatoric fabric.

2. DEM simulations

Three-dimensional simulations were conducted with a modified version of the open-source code LAMMPS (Plimpton, 1995). The particle size distribution (PSD) of the numerical assemblies (given in Fig. 1) approximates that of Toyoura sand (Huang et al., 2014a). An initially non-contacting cloud of 10,624 particles, enclosed by periodic boundaries, was generated and then isotropically compressed to various combinations of void ratio and stress state, as summarised in Table 1. The initial density was controlled by changing the inter-particle friction coefficient (μ) during the isotropic compression stage. After the target isotropic stress had been reached, the specimen was then subjected to numerical cycling until p' and the number of contacts became constant, indicating equilibrium. μ was subsequently changed to 0.25 which is the value used during shearing. Additional cycles were performed in order to ensure equilibrium before shearing was commenced. Four samples were created at confining pressures ranging from 100 kPa to 5000 kPa with the void ratio ranging from loose to medium dense.

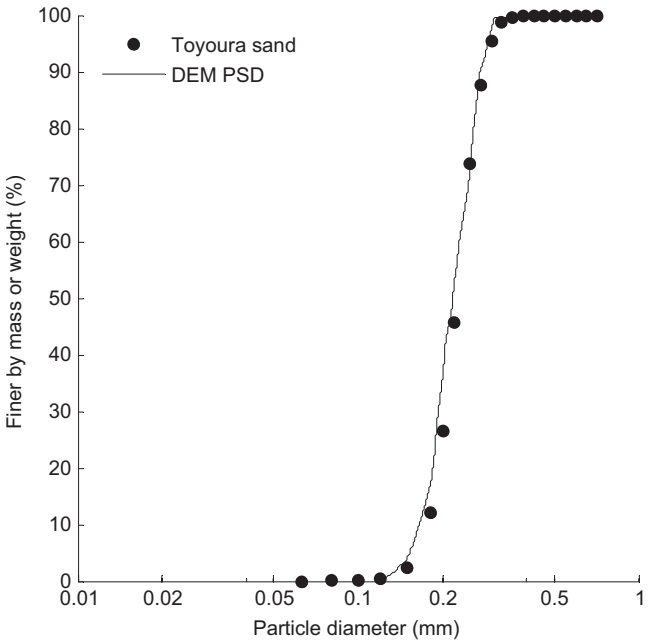

Fig. 1. Particle size distribution of numerical samples compared with laboratory data for Toyoura sand.

Following isotropic compression, the samples were sheared under constant p' conditions which gave a constant value for I

Table 1
Summary of constant-p' triaxial simulations.

p' (kPa)	e_0	Strain rate (1/s) , $d\varepsilon_1/dt$ and $d\varepsilon_3/dt$ for different I and p'											
		I=5e−1			I=1e−1			I=5e−2			I=1e−2		
		$d\varepsilon_1/dt$	min $d\varepsilon_3/dt$	max $d\varepsilon_3/dt$	$d\varepsilon_1$/dt	min $d\varepsilon_3/dt$	max $d\varepsilon_3/dt$	$d\varepsilon_1/dt$	min $d\varepsilon_3/dt$	max $d\varepsilon_3/dt$	$d\varepsilon_1/dt$	min $d\varepsilon_3/dt$	max $d\varepsilon_3/dt$
100	0.616	500.7	−898.1	−264.2	100.1	−182.3	−50.4	50.1	−88.6	−24.6	10.0	−18.1	−4.9
1000	0.611	1583.2	−2938.8	−830.8	316.6	−572.2	−153.8	158.3	−289.5	−77.0	31.7	−55.4	−15.3
2500	0.649	2503.3	−4488.4	−596.6	500.7	−858.1	−140.9	250.3	−430.7	−73.6	50.0	−89.2	−14.9
5000	0.596	3540.2	−6145.9	−1884.4	708.0	−1228.1	−358.2	354.0	−621.7	−178.6	70.8	−121.4	−35.9
		I=2.5e−3			I=1e−3			I=7.5e−4			I=5e−4		
		$d\varepsilon_1/dt$	min $d\varepsilon_3/dt$	max $d\varepsilon_3/dt$	$d\varepsilon_1$/dt	min $d\varepsilon_3/dt$	max $d\varepsilon_3/dt$	$d\varepsilon_1/dt$	min $d\varepsilon_3/dt$	max $d\varepsilon_3/dt$	$d\varepsilon_1/dt$	min $d\varepsilon_3/dt$	max $d\varepsilon_3/dt$
		2.5	−4.6	−1.2	1.0	−1.8	−0.5	0.8	−1.4	−0.4	0.5	−0.9	−0.2
		7.9	−13.4	−3.8	3.2	−5.8	−1.5	2.4	−4.1	−1.1	1.6	−2.9	−0.8
		12.5	−22.3	−3.8	5.0	−8.7	−1.5	3.8	−6.4	−1.1	2.5	−4.4	−0.8
		17.7	−30.1	−9.0	7.1	−12.4	−3.6	5.3	−9.1	−2.7	3.5	−6.1	−1.8

*$d\varepsilon_1/dt$ constant during shearing stage. **$d\varepsilon_3/dt$ variable during shearing stage.

throughout the shearing process, where I was calculated using the strain rate applied in the direction of the major principal stress ($\dot{\varepsilon}_1$). $\dot{\varepsilon}_1$ was specified to give eight different values for I ranging from 5e−4 to 5e−1, as shown in Table 1. A servo-control algorithm was implemented that determined the $\dot{\varepsilon}_3$ needed to maintain constant-p' conditions; and thus, $\dot{\varepsilon}_3$ varied during the shearing stage. The minimum and maximum strain rates in the direction of $\sigma'_3(\dot{\varepsilon}_3)$ are also included in Table 1. If $\dot{\varepsilon}_3$ were considered in the definition of I (i.e., the absolute value for $\dot{\varepsilon}_3$), it would not be possible to keep I constant throughout the shearing stage. In previous contributions (i.e., MiDi, 2004; da Cruz et al., 2005), the definition for shear rate corresponds to the strain rate in the loading direction ($\dot{\varepsilon}_1$), as is adopted in the present study. The loading conditions applied to the system are shown in Fig. 2. A simplified Hertz–Mindlin contact model was used with a shear modulus (G) of 29 GPa, a particle Poisson's ratio (ν) of 0.12, and particle density (ρ) of 2650 kg/m^3. A local damping coefficient of 0.1 was used in all the simulations and gravity was not considered in these periodic cell simulations.

The input values adopted for the shear modulus and Poisson's ratio are consistent with the range in elastic properties for quartz (Simmons and Brace, 1965). Similar values for Poisson's ratio have been used in other studies (Ng, 2009; Huang et al., 2014a). For real quartz particles, the friction values are in the range of 0.12–0.35, as was observed by Senetakis et al. (2013). Furthermore, it was reported by Huang et al. (2014b) that using an interparticle friction coefficient higher than 0.5, together with a simplified Hertz–Mindlin contact model, will result in a non-physical response.

One of the key assumptions of DEM simulations is that particles are treated as rigid bodies, which are allowed to overlap with other particles at the contact points. Therefore, all overlaps should be small in relation to the particle sizes; and thus, a maximum overlap ratio of 5% can be considered as an appropriate limit, as suggested by the Itasca Consulting Group (2007).

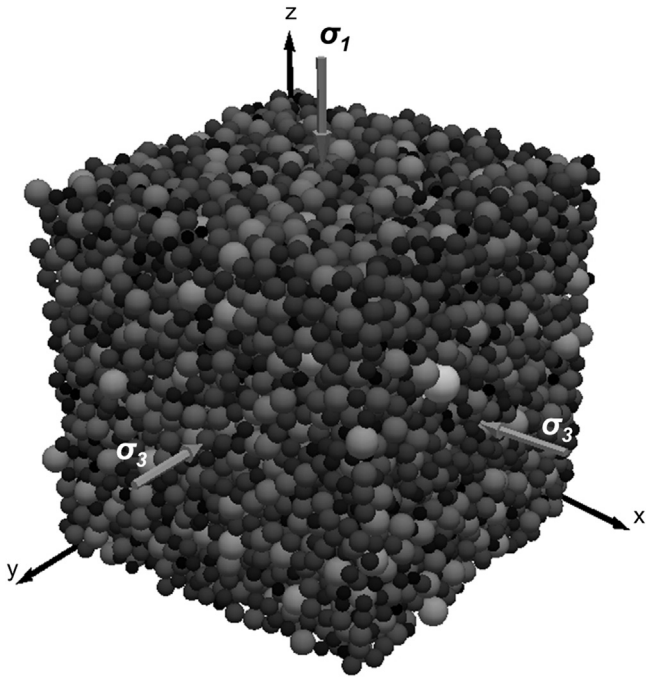

Fig. 2. Representative sample under loading conditions for constant p' simulations.

3. Overall response

Fig. 3(a) and (b) shows the variations in stress ratio $\eta=q/p'$ (q is the deviatoric stress) and volumetric strain ε_v, respectively, with the major principal strain (ε_1) for a representative set of simulations with p' =100 kPa and an initial void ratio (e_0) of 0.616. All of these simulations indicate a material response typically representative of dense or medium-dense samples. At a given strain level, both ε_v and η vary systematically with I. After an initial contraction during the first 5% of axial strain, samples sheared at higher strain rates (large I) tend to dilate more. For the case of I=5e−1, there

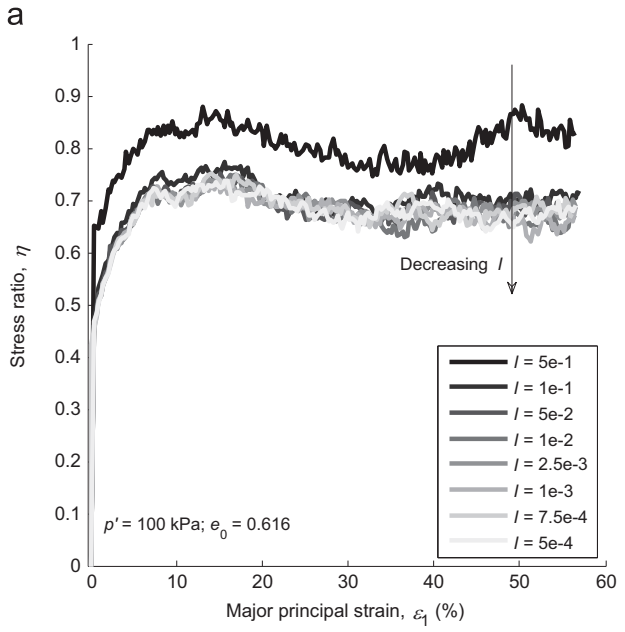

Stress ratio against major principal strain (p' = 100 kPa, e_0 = 0.616)

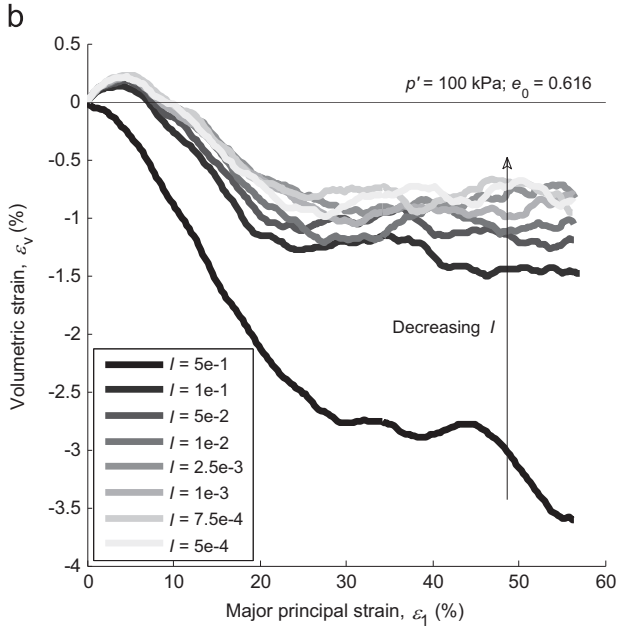

Volumetric strain against major principal strain (p' = 100 kPa, e_0 = 0.616)

Fig. 3. Overall response of the numerical sample for various values of I. (a) Stress ratio against major principal strain (p' = 100 kPa, e_0 = 0.616). (b) Volumetric strain against major principal strain (p' = 100 kPa, e_0 = 0.616).

is no initial contraction and the samples dilate throughout shearing. Samples sheared with $I \leq 2.5e-3$ give indistinguishable volumetric responses reaching the same value of ε_v at the critical state. Referring to Fig. 3(a), both the peak and critical state values for η decrease as I decreases. Although some fluctuations are present, samples sheared with $I \leq 2.5e-3$ show a very similar response in η both at the initial peak and at the critical state. A similar dependence of ε_v upon I was found for all other p' values. However, the response characteristics at higher stress levels were close to those of loose samples.

Fig. 4 presents the variation in η with dilatancy ($D = d\varepsilon_v/d\varepsilon_q$) for the case of p' = 100 kPa and e_0 = 0.616 in Fig. 4(a) and for the case of p' = 5000 kPa and e_0 = 0.596 in Fig. 4(b). D was calculated from the total strain using a central-difference approach (Been and Jefferies, 2004) and considering the elastic strain components to be negligible. The figures show a consistent response with higher η attained at negative values of dilatancy regardless of I. For the two levels of p' considered, the stress–dilatancy relationships are indistinguishable for simulations with $I \leq 2.5e-3$.

4. Critical state response

4.1. Macro-mechanical response

Fig. 5(a) illustrates the variation in the critical state η value with I; each η value was obtained from a set of five simulations, each set having different p' values. It is clear that when $I > 1e-2$, η increases as I increases; however, η is not sensitive to I for values of $I \leq 1e-2$. These data agree with prior 2D (da Cruz et al., 2005) and 3D planar shear simulations (Azema and Radjai, 2014). Fig. 5(b) shows the variation in e_{cs} (the void ratio at the critical state) with I for the p' values considered. For a given p', the value of e_{cs} remains almost constant when $I \leq 2.5e-3$. However, e_{cs} increases with I when $I > 2.5e-3$. Fig. 5(c) gives the $e_{cs} - (p'/p_a)^{0.7}$ relationship; the data for each I value are seen to follow the linear relationship suggested by Li and Wang (1998), i.e., $e_{cs} = \Gamma - \lambda (p'/p_a)^{\alpha}$, where Γ is the intercept of CSL, λ is the slope of the CSL, p_a is atmospheric pressure (101.325 kPa), and the α value of 0.7 suggested for Toyoura sand by Li and Wang (1998) is used. Note that each data point was taken as the averaged value for e and p' over the last 10–20% of axial strain due to the fluctuations in the load–deformation response. The CSLs move downwards with decreasing I when $I \geq 2.5e-3$, and the CSLs do not vary noticeably when $I \leq 2.5e-3$. The CSL parameters, Γ and λ, are presented in Fig. 5(d) for the different sets of simulations. Both Γ and λ decrease with I and constant values for Γ, and insignificant variations in λ can be observed for samples sheared at $I \leq 2.5e-3$.

4.2. Micro-mechanical response

In an attempt to understand the physical basis for the variation in sensitivity of the overall load–deformation response to I, two particle-scale parameters were analysed. The structural anisotropy (fabric), using the fabric tensor defined by Satake (1982), is

$$\Phi_{ij} = \frac{1}{N_c} \sum_{1}^{N_c} n_i n_j \tag{1}$$

where N_c is the total number of contacts and n_i is the unit contact normal. The largest, intermediate, and smallest eigenvalues of the fabric tensor are denoted as Φ_1, Φ_2, and Φ_3 respectively. The deviatoric fabric, $\Phi_1 - \Phi_3$, describes the degree of structural anisotropy. A second parameter is the mechanical coordination number (Z_m) defined as the average

number of contacts per particle excluding "rattlers" with zero or one contact (Thornton, 2000). As reported by Thornton (2000), samples at the same stress level with differing initial densities tend towards a unique Z_m at large strain levels. For this data set, $(\Phi_1-\Phi_3)$ tends towards a unique critical value at large strain levels; this is in line with the observations of Guo and Zhao (2013). Fig. 6(a) shows $(\Phi_1-\Phi_3)$ against Z_m at the critical state for different values of I. A linear relationship between $(\Phi_1-\Phi_3)$ and Z_m is observed in all cases of I. It is also evident in Fig. 6(a) that the loci move downwards with decreasing I, converging towards the same values at $I \leq 2.5e-3$. These data indicate that when the structural anisotropy is higher, fewer load-bearing contacts exist in the system. The product of $(\Phi_1-\Phi_3)$ and Z_m gives an indication of the intensity of the contacts acting in the orientation of the major fabric relative to that of the contacts oriented in the minor fabric direction (Maeda et al., 2010). Fig. 6(b) shows that this deviator fabric intensity depends on I. The data show that the deviator fabric intensity increases with I when $I \geq 1e-2$. A more constant response of the deviator fabric intensity ($Z_m^*(\Phi_1-\Phi_3)$), regardless of p', is observed when $I \leq 2.5e-3$ showing a critical state structure independent of the strain rate.

The connectivity, C, which reflects the number of contacts possessed by each particle (e.g., Shire and O'Sullivan, 2013) was also considered for all tests. The minimum value of C for a particle to be considered (statically) mechanically stable in a frictional system is four (Zhang and Makse, 2005). For this study, particles with $C \leq 3$ are considered unstable. Fig. 7(a) illustrates the frequency of C for various I with $p' = 100$ kPa and $e_0 = 0.616$. Fig. 7(b) shows the probability of the occurrence of unstable and stable particles against I for various values of p'. For $I > 2.5e-3$, the proportion of unstable particles increases with increasing I. The distribution of C values is not very sensitive to I for $I \leq 2.5e-3$. Thus, it seems that as I increases beyond $2.5e-3$, the mechanical redundancy of the system is diminished and more particles are accelerating (i.e., the unbalanced forces / inertial effects are no longer negligible); and thus, they are not in a state of static equilibrium.

5. Conclusions

This research has added to previous studies by considering the sensitivity of the material response to the inertial number (I) within the critical state soil mechanics framework. Thirty-two triaxial test simulations were performed in order to define an upper limit of I for quasi-static simulations independent of the strain rate. I has been systematically controlled by specifying different values for the mean effective stress (p') and strain rate ($\dot{\varepsilon}$), allowing the effect of I to be established. The data presented here can be used in DEM analyses to help make informed decisions about the appropriate strain rate for running DEM simulations of soil mechanics element tests.

A clear dependency of the dilatancy on I was found for $I > 1e-2$, while an indistinguishable response was observed for the cases of $I \leq 2.5e-3$. Considering the macro-mechanical critical state relationships, only those tests performed at values of $I \leq 2.5e-3$ showed a response which is independent of the strain rate (same CSL in the $e_{cs}-(p'/p_a)^{\alpha}$ plane). For higher I values, the CSL position depends on I. In terms of the micro-mechanical parameters, $(\Phi_1-\Phi_3)$ and Z_m, the samples again exhibited a response independent of the strain rate for values of $I \leq 2.5e-3$. The data plotted in the $(\Phi_1-\Phi_3)-Z_m$ plane showed a linear relationship. A critical

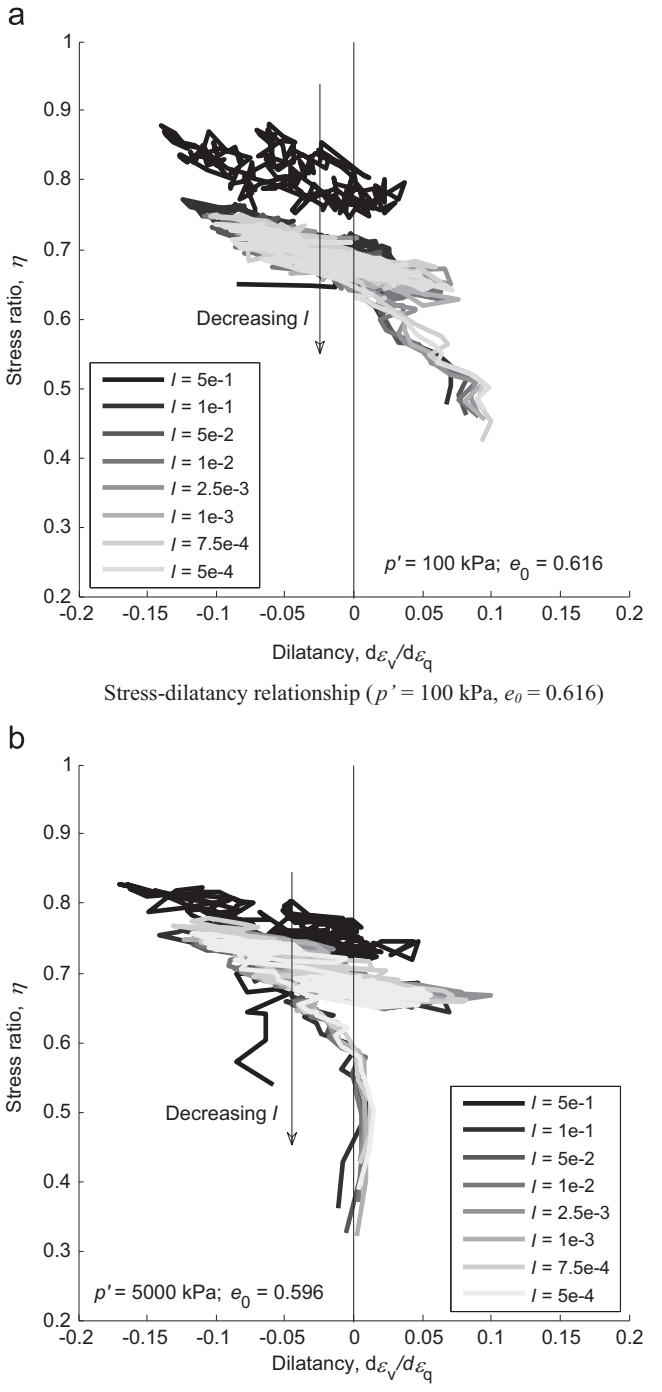

Fig. 4. Stress–dilatancy relationships (a) Stress-dilatancy relationship ($p' = 100$ kPa, $e_0 = 0.616$). (b) Stress-dilatancy relationship ($p' = 5000$ kPa, $e_0 = 0.596$).

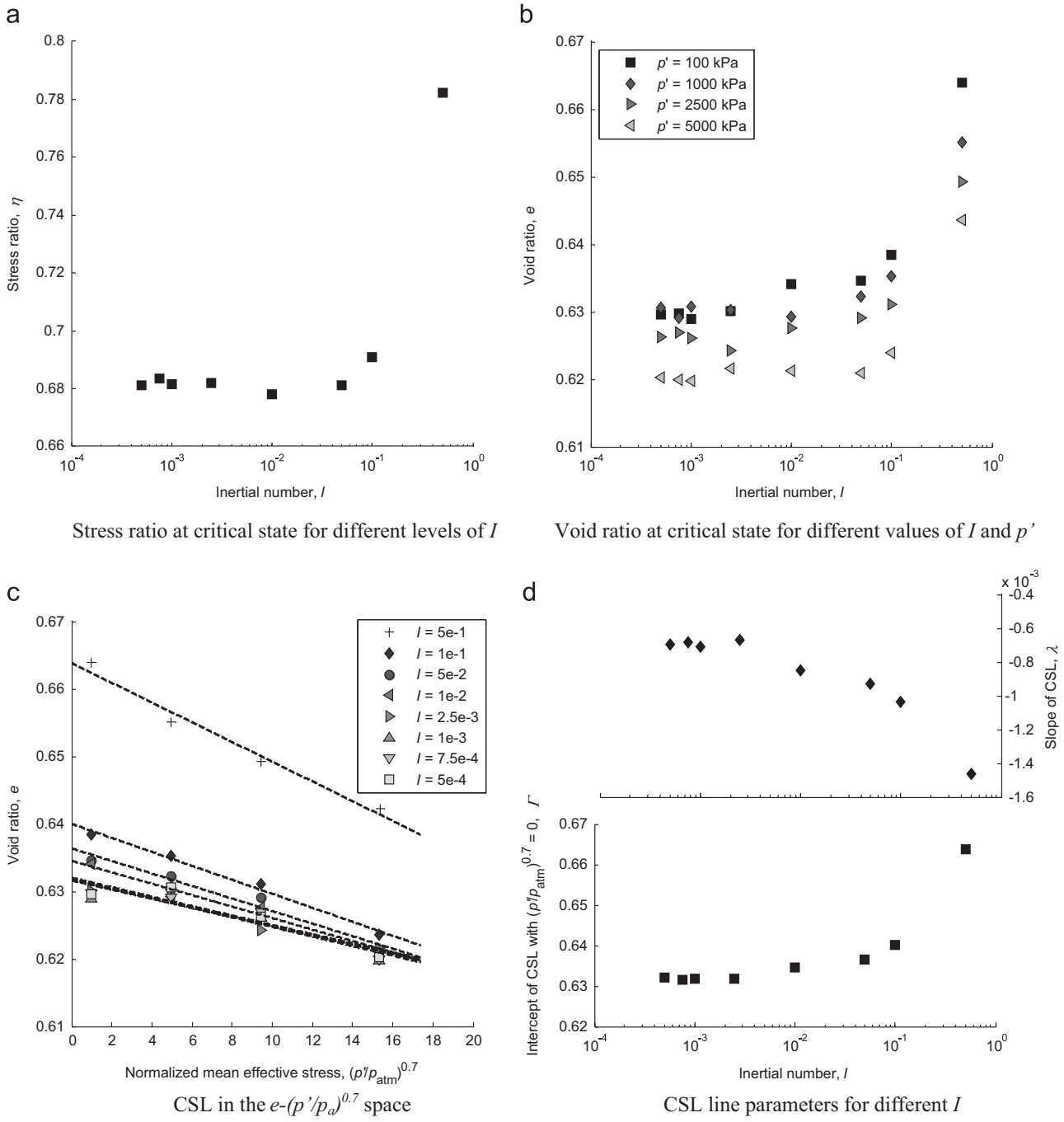

Fig. 5. Macro-scale analysis of the critical state (a) Stress ratio at critical state for different levels of I. (b) Void ratio at critical state for different values of I and p'. (c) CSL in the e-$(p'/p_a)^{0.7}$ space. (d) CSL line parameters for different I.

state structure, as noticed from the deviator fabric intensity, was also found to be independent of the strain rate from values of $I \leq 2.5e-3$. Similarly, there was a marked decrease in the number of particles that are statically redundant, i.e., that have four or more contacts when $I > 2.5e-3$.

From the above-described results, it is reasonable to propose a conservative upper limit for quasi-static simulations of $I = 2.5e-3$ that includes a strain-rate independent response from both macro- and micro-mechanical perspectives. This contribution has clearly demonstrated the sensitivity of the observed stress-deformation response to the applied strain rate in DEM simulations,while highlighting the usefulness of considering I as an indicator of quasi-static conditions when selecting a suitable strain rate. Choosing a strain rate based on I is more theoretically justifiable than a trial-and-error procedure that consists of varying the strain rate until a consistent response is achieved.

The upper limit proposed for quasi-static simulations is consistent with that found in some of the available literature (MiDi,

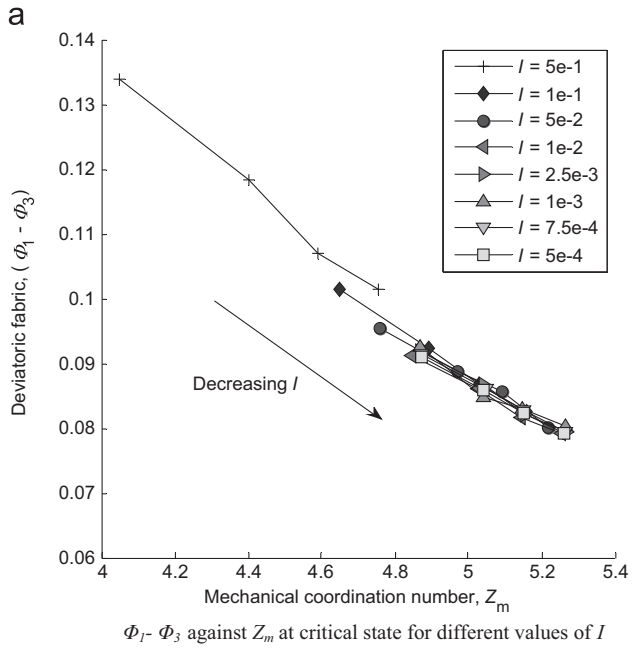

Φ_1- Φ_3 against Z_m at critical state for different values of I

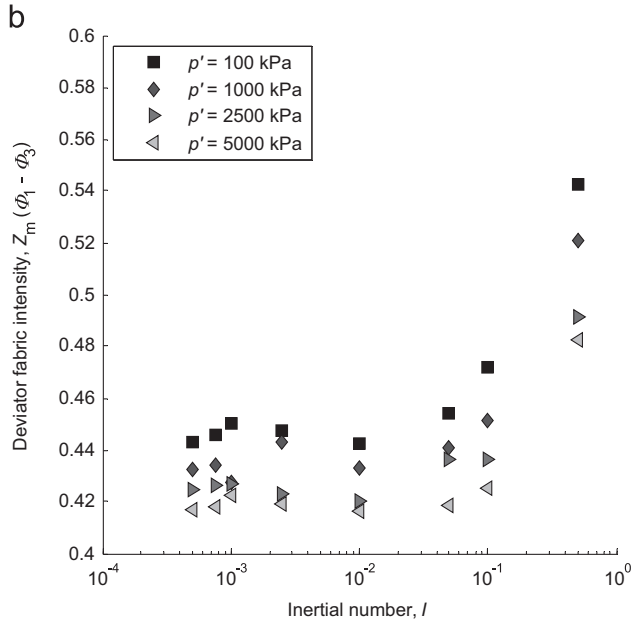

Fabric intensity at critical state against I for different values of p'

Fig. 6. h($\Phi_1-\Phi_3$)$-Z_m$ relationships at te critical state (a) Φ_1- Φ_3 against Zm at critical state for different values of I. (b) Fabric intensity at critical state against I for different values of p'.

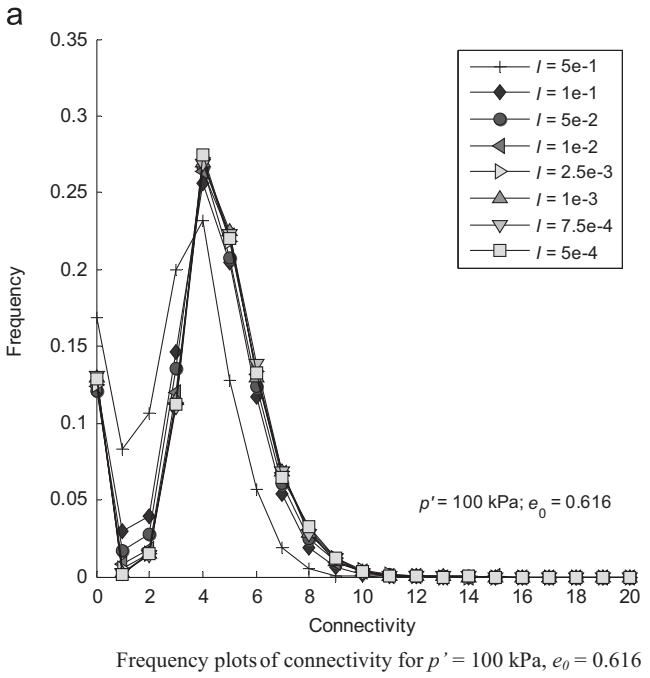

Frequency plots of connectivity for p' = 100 kPa, e_0 = 0.616

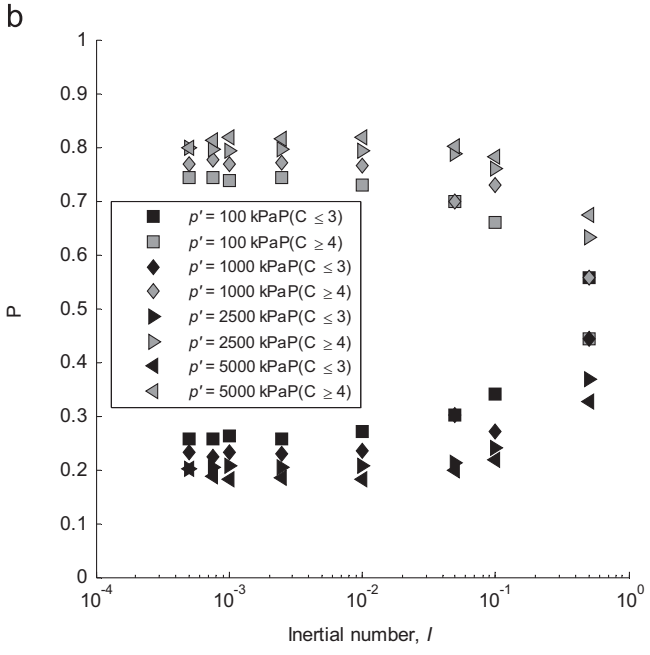

Probability of connectivity P($C \leq 3$) and P($C \geq 4$) for various p'

Fig. 7. Connectivity at the critical state. (a) Frequency plots of connectivity for p' = 100 kPa, e_0 = 0.616. (b) Probability of connectivity P($C \leq 3$) and P($C \geq 4$) for various p'.

2004; da Cruz et al., 2005; Koval et al., 2009; Azema and Radjai, 2014). This newly-acquired data, combined with the existing data in the literature, seems to indicate that the critical I proposed to maintain quasi-static conditions is independent of the initial density, the type of test, and the number of particles. For drained and constant volume tests, in which p', and consequently I, vary, attention should be paid so that the value of I does not exceed the limit proposed. Guo and Zhao (2014a, 2014b) chose a strain rate for DEM simulations by considering a value of I below the limit proposed in this study. As a guidance for conducting conventional triaxial tests using DEM, it is suggested that the strain rate applied in the direction of loading should be carefully chosen based on the $I \leq 2.5e-3$ criterion using the expected minimum p' (i.e., p'_0 in a conventional drained simulation or p' at the phase transformation for undrained simulations).

Acknowledgements

This research was supported and financed by The University of Hong Kong Seed Funding Programme for Basic Research.

The work presented in this study was conducted using the research computing facilities of the HKU Information Technology Services that are supported in part by the Hong Kong UGC Special Equipment Grant (SEG HKU09).

References

Agnolin, I., Roux, N.J., 2007. Internal states of model isotropic granular packings. I. Assembling process, geometry, and contact networks. Phys. Rev. E 76, 061302.

Azema, E., Radjai, F., 2014. Internal structure of inertial granular flows. Phys. Rev. Lett. 12, 078001.

Been, K., Jefferies, M., 2004. Stress–dilatancy in very loose sand. Can. Geotech. J. 41, 972–989.

Cundall, P.A., Strack, O.D.L., 1979. A discrete element model for granular assemblies. Geotechnique 29 (1), 47–65.

da Cruz, F., Emam, S., Prochnow, M., Roux, J.N., Chevoir, F., 2005. Rheophysics of dense granular materials: discrete simulation of plane shear flows. Phys. Rev. E 72, 021309.

Gimbert, F., Amitrano, D., Weiss, J., 2013. Crossover from quasi-static to dense flow regime in compressed frictional granular media. EPL 104, 46001.

Guo, N., Zhao, J., 2013. The signature of shear-induced anisotropy in granular media. Comput. Geotech. 47, 1–15.

Guo, N., Zhao, J., 2014a. Local fluctuations and spatial correlations in granular flows under constant-volume quasi-static shear. Phys. Rev. E 89, 042208.

Guo, N., Zhao, J., 2014b. A coupled FEM/DEM approach for hierarchical multiscale modelling of granular media. Int. J. Numer. Methods Eng. 99, 789–818.

Hanley, K.J., Huang, X., O'Sullivan, C., Kwok, C.Y., 2013. Challenges of simulating undrained tests using the constant volume method in DEM. AIP Conf. Proc. 1542, 277.

Hatano, T., 2007. Power-law friction in closely packed granular materials. Phys. Rev. E 75, 060301.

Huang, X., O'Sullivan, C., Hanley, K.J., Kwok, C.Y., 2014a. DEM analysis of the state parameter. Géotechnique 64 (12), 954–965.

Huang, X., Hanley, K.J., O'Sullivan, C., Kwok, C.Y., 2014b. Exploring the influence of interparticle friction on critical state behaviour using DEM. Int. J. Numer. Anal. Methods 38 (12), 1276–1297.

Itasca Consulting Group, 2007. PFC3D Version 4.0 User Manual. Itasca Consulting Group, Minneapolis, MN, USA.

Koval, G., Roux, J.N., Corfdir, A., Chevoir, F., 2009. Annular shear of cohesionless granular materials: from the inertial to quasistatic regime. Phys. Rev. E 79, 021306.

Kuwano, O., Ando, R., Hatano, T., 2013. Granular friction in a wide range of shear rates. AIP Conf. Proc. 1542, 32.

Li, X.S., Wang, Y., 1998. Linear representation of steady-state line for sand. J. Geomech. Geoenviron. Eng. 124, 1215–1217.

Macaro, G., Utili, S., 2012. DEM triaxial tests of a seabed sand. Discrete Element Modelling of Particulate Media. The Royal Society of Chemistry 203–211.

Maeda, K., Sakai, H., Kondo, A., Yamaguchi, T., Fukuma, M., Nukudami, E., 2010. Stress-chain based micromechanics of sand with grain shape effect. Granul. Matter 12, 499–505.

MiDi, G.D.R., 2004. On dense granular flows. Eur. Phys. J. E 14, 341–365.

Ng, T., 2009. Discrete element method simulations of the critical state of a granular material. Int. J. Geomech. 9 (5), 209–216.

Peyneau, P.E., Roux, J.N., 2008. Frictionless beads packs have macroscopic friction, but no dilatancy. Phys. Rev. E 78, 011307.

Plimpton, S., 1995. Fast parallel algorithms for short-range molecular dynamics. J. Comput. Phys. 117, 1–19.

Radjai, F., Dubois, F., 2011. Discrete-Element Modelling of Granular Materials. ISTE, London.

Satake, M., 1982. Fabric tensor in granular materials. In: Vermeer, P.A., Luger, H.J. (Eds.), Proceedings of the IUTAM Symposium on Deformations and Failure of Granular, Balkema, Rotterdam, pp. 63–68.

Senetakis, K., Coop, M.R., Todisco, M.C., 2013. Tangential load–deflection behaviour at the contacts of soil particles. Géotech. Lett. 3 (2), 59–66.

Shire, T., O'Sullivan, C., 2013. Micromechanical assessment of an internal stability criterion. Acta Geotech. 8 (2013), 81–90.

Simmons, G., Brace, W.F., 1965. Comparison of static and dynamic measurements of compressibility of rocks. J. Geophys. Res. 70 (22), 5649–5656.

Thornton, C., 2000. Numerical simulations of deviatoric shear deformation of granular media. Géotechnique 50 (1), 43–53.

Zhang, H.P., Makse, H.A., 2005. Jamming transition in emulsions and granular materials. Phys. Rev. E 72, 011301.